Published in final edited form as:
Biochemistry. 2011 October 4; 50(39): 8463–8477. doi:10.1021/bi201007t.

Hidden in Plain Sight: Subtle Effects of the 8-Oxoguanine Lesion on the Structure, Dynamics, and Thermodynamics of a 15-Base-Pair Oligodeoxynucleotide Duplex†

Charisse M. Crenshaw[£], **Jacqueline E. Wade**[§], **Haribabu Arthanari**[Ω], **Dominique Frueh**[β], **Benjamin F. Lane**[¢], and **Megan E. Núñez**[§,*]

[§]Department of Chemistry, Mount Holyoke College, South Hadley, Massachusetts 01075

[£]Department of Molecular and Cellular Biology, Harvard University, Cambridge MA 02138

[Ω]Department of Biological Chemistry and Molecular Pharmacology, Harvard Medical School, Boston MA 02115

[β]Department of Biophysics and Biophysical Chemistry, Johns Hopkins University School of Medicine, Baltimore MD 21205

[¢]Charles Stark Draper Laboratory, Cambridge MA 02139

Abstract

The base lesion 8-oxoguanine is formed readily by oxidation of DNA, potentially leading to G→T transversion mutations. Despite the apparent similarity of 8-oxoguanine-cytosine base pairs to normal guanine-cytosine base pairs, cellular base excision repair systems effectively recognize the lesion base. Here we apply several techniques to examine a single 8-oxoguanine lesion at the center of a nonpalindromic 15-mer duplex oligonucleotide in an effort to determine what, if anything, distinguishes an 8-oxoguanine-cytosine base pair from a normal base pair. The lesion duplex is globally almost indistinguishable from the unmodified parent duplex using CD spectroscopy and UV melting thermodynamics. The DNA mismatch-detecting photocleavage agent $Rh(bpy)_2chrysi^{3+}$ cleaves only weakly and nonspecifically, revealing that the 8oxoG-C pair is locally stable at the level of the individual base pairs. NMR spectra are also consistent with a well-conserved B-form duplex structure. In the 2D NOESY spectra, base-sugar and imino-imino crosspeaks are strikingly similar between parent and lesion duplexes. Changes in chemical shift due to the 8oxoG lesion are localized to its complementary cytosine and to the 2–3 base pairs immediately flanking the lesion on the lesion strand. Residues further removed from the lesion are shown to be unperturbed by its presence. Notably, imino exchange experiments indicate that the 8-oxoguanine-cytosine pair is strong and stable, with an apparent equilibrium constant for opening equal to that of other internal guanine-cytosine base pairs, on the order of 10^{-6}. This collection of experiments shows that the 8-oxoguanine-cytosine base pair is incredibly stable and similar to the native pair.

†This work was supported by the Camille and Henry Dreyfus Foundation, the Clare Boothe Luce Foundation, the Radcliffe Institute for Advanced Study at Harvard University, and the National Institutes of Health/NIGMS (1R15GM083250).

*To whom correspondence should be addressed: Department of Chemistry, 50 College Street, Mount Holyoke College, South Hadley, MA 01075. Telephone: (413) 538-2449; Fax: (413) 538-2327; menunez@mtholyoke.edu.

Supporting Information Available

Supplemental information, including structures of normal and lesion base pairs, tables of mixing times, melting temperature curves, annotated NOESY spectra, tables of chemical shift assignments, representative Matlab fits, and comparisons of exchange rates between normal and lesion duplexes, is available free of charge via the internet at http://www.pubs.acs.org.

DNA is constantly being damaged by endogenous and exogenous agents (1). Damage to the DNA bases is particularly insidious because the information content of the sequence may be lost if the base is modified; if left unrepaired, covalent chemical changes to the DNA structure can lead to mutations and ultimately to cancinogenesis or apoptosis. One of the most common damage lesions in DNA is 8-oxo-7,8-dihydro-2'-deoxyguanosine (8-oxoguanine or 8oxoG), which can be readily generated by a range of oxidants and reactive species via a variety of mechanisms due to guanine's low redox potential (2–4). If not removed, the replicative DNA polymerases frequently pair 8oxoG with an incoming adenine, leading to a G to T transversion mutation (5, 6).

The 8oxoG nucleotide is chemically similar to its parent guanine. The transformation from normal base to lesion occurs via the replacement of a hydrogen at C8 with a keto group and protonation of the N7 lone pair, both at positions facing into the major groove (Supp. Fig.1). Two consequences of the oxidation are a shift in the pK_a of the N1 imino nitrogen of approximately −0.7 pH units relative to normal guanine and a rotation of the base dipole by 42° (7, 8). Nonetheless, the size of the base is very similar to the parent guanine, the lesion base remains aromatic and planar, and its Watson-Crick hydrogen-bonding edge is unchanged (9).

Both NMR (10) and X-ray crystallographic (11) studies of the 8oxoG lesion paired with cytosine in a duplex DNA showed the B-form DNA duplex structure to be maintained. Base stacking, base pairing, and helical twist are unperturbed, even in the vicinity of the lesion. The 8oxoG stacks normally within the helix in the *anti* conformation and forms Watson-Crick hydrogen bonds to its cytosine pair. More recent structures of three duplexes containing 8oxoG, co-crystallized with a protein scaffold, show the sugar pucker to be C2'-*endo* at the lesion nucleoside consistent with canonical B-form DNA (12). Only when paired with adenine does 8oxoG adopt the *syn* conformation to form a Hoogsteen base pair, but even in this case the overall helical geometry is surprisingly well-conserved (13, 14).

Other data support this picture of the 8oxoG-C pair as subtle and nondisruptive to B-form DNA conformation. The substitution of 8oxoG for G in a 13-mer oligonucleotide duplex resulted in a small $\Delta\Delta G$ for the duplex-single strand equilibrium of $+2.0 \pm 0.7$ kcal/mol (15). This modest loss of free energy is due to a more substantial loss in enthalpy that is somewhat counterbalanced by a gain in entropy. Computational studies of 8oxoG paired with cytosine in a DNA duplex predict a variety of small changes in the structure, flexibility, and stability of the helix (16–19).

Though DNA containing an 8oxoG-C base pair is clearly quite similar to that containing an undamaged Watson-Crick pair, multiple repair enzymes have evolved to detect and remove the lesion base from DNA, including the bacterial MutM (Fpg) glycosylase and the mammalian OGG (20). These enzymes selectively detect relatively rare 8oxoG lesions in a sea of normal guanine bases despite the lesion's camouflaged appearance, leading to the question of how base excision repair (BER) glycosylases find their targets (20, 21). Work with uracil DNA glycosylase, another BER glycosylase, suggests that the enzyme "catches" a uracil base when it is spontaneously extruded from the helix, stabilizing the open state by slowing the rate of closing but not actively causing it to form (22, 23). Conversely, crystallographic and computational work with MutM suggests that this enzyme subtly deforms the DNA as it scans for lesions in order to selectively destabilize the 8oxoG lesion, catalyzing its extrusion (24). The extent to which repair enzymes can capitalize upon inherent differences between 8oxoG and G in double stranded DNA, as opposed to actively probing and perturbing the DNA, remains unclear. If the 8oxoG-C base pair is locally less stable than the normal G-C base pair, with distinctly different rates of base pair opening or

closing or a shift in the base pair opening equilibrium toward an open state, the 8oxoG lesion might in effect signal for its own repair.

To explore further the question of whether or not the 8oxoG-C base pair is more destabilized and open than a normal G-C pair, we have used a variety of methods to explore sensitively its structure, thermodynamics, and base pair opening equilibrium. Our experimental DNA duplex is a nonpalindromic 15 bp oligonucleotide containing a single centrally-placed lesion. The size of our construct, larger than in other structural studies, allows for examination not only the lesion base pair and its immediate flanking bases, but also of several base pairs further away from the lesion. The choice of a non-palindromic sequence, while experimentally more challenging, allows us to exclude possible cooperative effects due to two lesions in close proximity. By bringing several methods to bear on the same duplex sequence for the first time, we demonstrate that the effects of 8oxoG are extremely subtle and localized to the immediate vicinity of the lesion.

Materials and Methods

Preparation of DNA, Buffers, and Catalyst

All DNA oligonucleotides were prepared by automated phosphoramidite synthesis, purified by PAGE or HPLC, and characterized by mass spectrometry, either in the Verdine laboratory at Harvard University or commercially (Midland Certified Reagent Company and Integrated DNA Technologies). Residual salts were removed by purification of the DNA through Sep-Pak reverse phase cartridges (Waters Corporation, Milford MA) and extensive dialysis against 1X NMR buffer, where 1X NMR buffer contains 10 mM sodium phosphate pH 7.5 and 100 mM NaCl. The concentration of DNA strands was determined spectrophotometrically using the following molar extinction coefficients: ε_{260} is 139,700 $M^{-1}cm^{-1}$ for strand **1**; 133,400 $M^{-1}cm^{-1}$ for strand **1oxo**; and 144,000 $M^{-1}cm^{-1}$ for strand **2**. Strands were annealed by mixing equimolar amounts of each strand to a final concentration between 650 – 700 μM duplex, heating to 90°C, and cooling gradually to 4°C. D_2O was added to the imino exchange samples to a final concentration of 5% for the purposes of the NMR lock.

Concentrated stocks of the deuterated glycine exchange catalyst were prepared at pH 7.5 to match the sample buffer pH and were added directly to the NMR tube. According to the Henderson-Hasselbach equation and an estimated pK_a of 10.2 at 8°C, the ratio of glycine present in its active form (i.e. with a deprotonated terminal amine group) to inactive zwitterion at this pH is 1:400.

Circular Dichroism Spectropolarimetry

DNA samples were prepared to an 8 μM concentration of each DNA strand in 1X NMR buffer. CD spectra were measured on a Jasco J-715 spectropolarimeter at 10°C using a 0.1 cm pathlength cell. Spectra were recorded between 220 and 320 nm at 0.2 nm increments with a scan rate of 20 nm/min. After subtracting the buffer blank and correcting for the molar nucleotide concentration and path length, the spectra were normalized to units of molar ellipticity to facilitate comparisons with spectra in the published literature (25).

Spectrophotometric Measurements of DNA Melting Thermodynamics

DNA duplexes were annealed to a concentration of 0.8 to 21 μM in 1X NMR buffer by heating to 80°C and cooling gradually to 4°C. Samples were degassed at 4°C to prevent formation of bubbles and were placed in cuvettes with a pathlength appropriate to give an absorbance at 260 nm of approximately 0.5 (0.1 cm, 0.2 cm, 0.5 cm, or 1 cm). The absorbance at 260 nm was measured as a function of temperature in a Varian Cary 50 UV-

visible spectrophotometer with a Peltier temperature-controlled cell. The absorbance was measured every 0.1 min while the temperature was ramped upward at 0.5°C/min between 8 and 80°C. The melting temperature or T_m, defined here as the inflection point of the temperature versus absorbance curve, was determined from the first derivative. At least three independent measurements were made at each of the five concentrations for each duplex.

The T_m values and concentrations were used to determine the change in enthalpy and entropy for the formation for each duplex using a form of the van't Hoff equation:

$$\frac{1}{T_m} = \frac{R(\ln C_{tot})}{\Delta H} + \frac{(\Delta S - 1.39R)}{\Delta H} \quad \text{(Eqn. 1)}$$

C_{tot} is the total concentration of DNA strands, which is twice the duplex concentration. A plot of $1/T_m$ versus $\ln C_{tot}$ is a straight line whose slope and intercept are used to determine the change in enthalpy and entropy associated with duplex formation. The change in Gibbs free energy associated with duplex formation was calculated from the change in enthalpy and entropy at 25°C.

Cleavage of DNA using $Rh(bpy)_2(chrysi)^{3+}$

DNA samples were annealed to an 8 μM duplex concentration with trace amounts of DNA containing a ^{32}P labeled phosphate at the 5' end. Experimental samples contained either 5 or 10 μM $Rh(bpy)_2(chrysi)^{3+}$ as described in the figure 2 legend. Dark control samples contained 10 μM rhodium complex, and light control samples contained no $Rh(bpy)_2(chrysi)^{3+}$. All samples except the dark controls were irradiated simultaneously in closed 1.7 mL plastic microcentrifuge tubes placed directly on top of a visible light box for 10 hours. After irradiation, samples were dried under vacuum in the dark, resuspended in denaturing running dye, heated briefly on a heat block at 90° C, and loaded directly onto a preheated 18% denaturing polyacrylamide gel (26). The location of cleavage was confirmed by comparison to Maxam-Gilbert purine-specific reaction controls (not shown). Gels were digitized by phosphorimagery on a Molecular Dynamics Storm 820 system (Amersham Biosciences), and band intensities were analyzed in ImageQuant software.

1D and 2D NMR Spectra

1D ^1H spectra were obtained at Harvard University on a Bruker AVANCE 700 MHz NMR equipped with a 5mM CPTCI cryogenic probe. Water suppression achieved using DANTE-based excitation sculpting with a W5 block (27). 1D spectra were recorded at 8°C on samples containing either no catalyst (duplex**1–2**) or 0.0125 mM catalyst (duplex **oxo1–2**).

2D NOESY (28, 29) experiments were performed at Harvard Medical School on a Bruker 750 MHz NMR equipped with a triple resonance TXI cryogenic probe. Two spectra were recorded for each sample. In both cases, the mixing time was 250 ms. The first NOESY spectrum was recorded in 95% H_2O/5% D_2O at 10°C. The spectral dimensions were 20 ppm (^1H, 2048 complex points) by 10 ppm (^1H, 500 complex points). 64 scans were accumulated with a recycling delay of 1 s. A second spectrum was recorded in 100% D_2O at 25°C. The spectral dimensions were 10 ppm (^1H, 2048 complex points) by 10 ppm (^1H, 600 complex points). 32 scans were accumulated with a recycling delay of 1 s. Spectra were processed with NMRPipe (30). They were superimposed, their resonances assigned, and their chemical shifts measured in Sparky (31) according to the NOE walk method (32–34). In the absence of COSY experiments, H4' and H5' protons were not assigned. A model of duplex **1–2** was created using Nucleic Acid Builder written by the Case group at Rutgers University (35).

The model was utilized in iMol without further refinement or structural modification purely for the purposes of visualization.

Measurement of Base Pair Opening by NMR

To monitor the exchange of imino protons and by extension to quantify base pair opening, we used magnetization inversion transfer from water protons as described by Guéron and Leroy (36). Imino exchange experiments were performed on a Bruker AVANCE 700 MHz NMR with a 5mM CPTCI cryogenic probe at Harvard University or on a Bruker 600 MHz NMR with a TCI cryogenic probe at the University of Massachusetts at Amherst. In short, inversion of the water proton magnetization was accomplished via a DANTE pulse scheme, magnetization transfer occurred during a mixing time (t_{mix}), and a jump-and-return sequence was used to suppress the water resonance (37, 38). Gradients were also included in the pulse sequence to suppress the transverse components of the solvent magnetization and reduce radiation damping (36). All spectra were taken at 8°C, and the temperature was calibrated before each run using the chemical shifts of a methanol standard (39, 40).

In order to measure the exchange rate of the imino protons, we first defined the parameters for water inversion and relaxation for each combination of sample and instrument. The efficiency of water inversion (E) was determined by integrating the area under the water peak for samples with and without a DANTE inversion (W_{inv} and W_{eq}, respectively):

$$E = 1 - \frac{W_{inv}}{W_{eq}} \quad \text{(Eqn. 2)}$$

E, determined independently for each data set, was always between 1.90 and 2.00. An apparent longitudinal relaxation rate for water, $R_{1w} = 1/(T_{1w})$, was measured by inversion recovery with the same pulse sequence used for the imino exchange measurements, in which the jump and return was replaced by an excitation pulse. This ensured that the resulting water relaxation rate described the behavior of water during the imino exchange experiment and accounts for the DANTE inversion and gradients. The water signal intensity W_z was then measured as a function of t_{mix}:

$$W_z(t_{mix}) = W_{z,eq}(1 - E \times e^{-t_{mix}R_{1w}}) \quad \text{(Eqn. 3)}$$

Fourteen spectra were obtained with mixing times ranging between 1.2 ms and 15 s (Supp. Table 1). The water relaxation curve was not exactly exponential due to residual radiation damping, so the nonlinear least-squares fit value of R_{1w} was determined independently for each sample and instrument between 1.2 ms and 2 s to match the time window sampled in the exchange experiment. R_{1w} was equal to 0.15–0.16 on the 700 MHz spectrometer and 0.30–0.40 on the 600 MHz spectrometer.

Imino exchange rates were obtained by magnetization inversion transfer at twenty-two different mixing times between 520 μs and 2 s (Supp. Table 2). The NMRPipe suite of programs (30) was used to uniformly zero fill, Fourier transform, phase, crop, and apply a 1st order baseline to each group of twenty-two spectra, as well as to establish the approximate chemical shift of each peak. Matlab (MathWorks, Natick MA) was used to deconvolute overlapping peaks in the spectrum and determine exchange and relaxation times. First, spectra were aligned by cross-correlation along the chemical shift axis, and the height of each peak was determined at each time point. The peak heights as a function of time were used to estimate the exchange rate for each imino peak (k_{ex}) by nonlinear least squares fitting to equation 4:

$$\frac{I_z(t_{mix})}{I_{z,eq}} = 1 + E \times k_{ex} \times (e^{-R_{1i}t_{mix}} - e^{-R_{1w}t_{mix}}) \quad \text{(Eqn. 4)}$$

E and R_{1w} were determined as described above, $I_z(t_{mix})$ and $I_{z,eq}$ were the measured intensities of the imino peaks after time t_{mix} or at equilibrium. The exchange rate k_{ex} and R_{1i} (which represents a combination of the imino proton relaxation rate and the chemical exchange rate k_{ex}) were determined by fitting equation 4 to the data. To refine parameter estimates for overlapping peaks, these values of k_{ex} and R_{1i} were then used to seed a multiparameter non-linear least-squares fit of a set of Lorentzian peaks to all twenty-two spectra simultaneously. The fit was implemented in Matlab using the *nlinfit* function. Each of the peaks was modeled using 5 free parameters (chemical shift, linewidth, intensity (volume), R_{1i} and k_{ex}).

Over a wide range of catalyst concentrations, the relationship between the rate of exchange (k_{ex}) and the catalyst concentration ([B]) can be described by

$$\frac{1}{k_{ex}} = \tau_{ex} = \frac{1}{k_{op}} + \frac{k_{cl}}{\alpha k_{op}(k_B[B] + k_{\text{int}})} \quad \text{(Eqn. 5)}$$

where k_{int} is the uncatalyzed intrinsic rate of exchange of the imino proton and α is a constant that reflects the accessibility of the imino proton to the catalyst (probably ~ 0.1 for glycine) (22, 41). k_{op} and k_{cl} are the rate of base pair opening and closing respectively. The ratio between k_{op} and k_{cl} gives the apparent equilibrium constant for base pair opening

$$\alpha K_{op} = \frac{k_{op}}{k_{cl}} \quad \text{(Eqn. 6)}$$

k_B is a second-order rate constant for base catalysis, a constant that can be directly calculated for each type of imino proton:

$$k_B = \frac{k_D}{(1 + 10^{pK_a^{nu} - pK_a^B})} \quad \text{(Eqn. 7)}$$

With a biomolecular collision rate k_D approximately equal to 0.47×10^9 M^{-1} s^{-1}, the k_B of DNA nucleotides in glycine buffer was calculated to be 3.1×10^8 M^{-1} s^{-1} for thymine, 3.9×10^8 M^{-1} s^{-1} for guanine, and 4.5×10^8 M^{-1} s^{-1} for 8oxoG (the latter based on an assumed pK_a 0.70 pH units lower than G at the same temperature) (7, 36).

According to Eqn. 5, a plot of the inverse of the base concentration versus the inverse of the exchange rate gives a curve such that at low concentrations, the measured rate of exchange reflects the intrinsic rate of exchange k_{int} of the imino proton by other weak bases in its environment (most likely its complementary nucleotide and surrounding nucleotides); at infinitely high concentrations, the rate of exchange approaches the rate of opening k_{op}. At very low catalyst concentrations similar to those used here, the apparent equilibrium constant for base pair opening αK_{op} and the intrinsic rate of exchange k_{int} can be determined from a plot of the k_{ex} versus [B] according to the following simplified linear relationship as described by Every and Russu (42):

$$k_{ex}=\alpha K_{op}(k_{int}+k_{\beta}[B]) \quad \text{(Eqn. 8)}$$

The exchange data between 5 mM and 600 mM glycine were fit to this equation in Gnuplot to give best-fit values of k_{int} and αK_{op} together with their associated uncertainties.

Results

The 15-mer DNA duplexes used in these studies are shown in Table 1. Duplex **1–2** (the undamaged control parent duplex) and duplex **1oxo-2** are identical except for the presence of the 8oxoG lesion at position 8. Unlike the duplexes used in the original NMR and X-ray structural studies of 8oxoG-C in DNA (10, 11), this sequence is not palindromic and contains a single lesion, allowing us to examine longer-range effects on the seven base pairs flanking the lesion on either side.

Effect of the 8oxoG Lesion on Duplex Stability, Global Structure, and Thermodynamics

We used three established techniques to confirm the formation of stable, B-form double helices by strands **1** and **2** (parent duplex) and **1oxo** and **2** (lesion duplex), and to assess the similarity between the two duplexes: circular dichroism spectropolarimetry (CD), UV melting thermodynamic measurements, and cleavage by $Rh(bpy)_2(chrysi)^{3+}$.

The circular dichroism spectra of both parent and lesion duplexes have maxima around 275 nm, minima around 248 nm, and a crossover point around 261 nm, consistent with the 15-mer oligonucleotides forming a B-form DNA double helix (Fig. 1a) (43–45). Both spectra are distinctly different from a single-stranded control, but are almost identical to one another between 220 and 320 nm.

The UV melting curves for the parent and lesion duplexes are also quite similar to one another, both in shape and in inflection point, though the lesion duplex shows a more gradual pre-melting transition (Supp. Fig 2). Generally the 8oxoG lesion causes the melting temperature (T_m) of this 15-mer duplex to decrease by only ~1° at any given concentration. When these measured T_m values are plotted as a function of duplex concentration (Fig. 1b), the thermodynamic parameters ΔH, ΔS, and ΔG can be determined using the van't Hoff relationship (Eqn. 1). In this 15-mer duplex, the loss in the change in the free energy of duplex formation due to the 8oxoG lesion (ΔΔG) is +0.4 ± 1.1 kcal/mol (Fig. 1c; Supp. Table 3).

$Rh(bpy)_2(chrysi)^{3+}$ is a water-soluble, cationic transition metal complex that has been shown to bind selectively by insertion of its large chrysi ligand into destabilized regions of the DNA double helix, in particular to base mismatches, and to cleave the DNA backbone at these sites upon photoexcitation with visible light (46, 47). When incubated and photoirradiated with the parent duplex **1–2**, the complex cleaves quite weakly, i.e. ~1% of strands after 10 hours of irradiation on a visible light box (Fig. 2). Cleavage in the parent duplex occurs predominantly at pyrimidines, specifically C_5 and somewhat less at C_{10} and T_{11} on the primary strand **1**, and at C_{23} and C_{25} on the complementary strand **2** (lanes 1, 2, and 9, 10 respectively). This cleavage is both rhodium- and light- dependent, as it occurs in neither the light or dark control lanes (lanes 3, 4, 11, 12). Interestingly, the pattern of cleavage does not change with the substitution of 8oxoG at position 8 of strand **1** (lanes 5, 6, 13,14). The intensity of photocleavage increases quite modestly at C_{23} and C_5 in the 8oxoG duplex (~20–40%), while cleavage at C_{25} remains relatively unchanged. Replacement of C_{23} by an adenine in strand **2** to create a G-A or 8oxoG-A mispair at the 8 position (lanes

17–24) does not increase chrysi photocleavage appreciably at this site, at least not on the primary strand.

Effect of the 8oxoG Lesion on Duplex Structure

Two dimensional Nuclear Overhauser Effect Spectroscopy (NOESY) was also utilized to evaluate the effect of the 8oxoG lesion on duplex structure. Because of the ordered and highly predictable structure of the double-stranded DNA polymer, most of the DNA duplex protons in a NOESY spectrum can be routinely assigned without additional spectra or specific labels (32–34). By "walking" down each strand consecutively and using a general knowledge of DNA structure, we could assign the H1', H2', and H2" sugar protons as well as most of the base protons (aromatic, imino, cytosine amino, and thymine methyl) and those H3' protons that were not overwhelmed by the water resonance.

The NOESY spectra of the 8oxoG lesion duplex were assigned using this series of NOE walks and known interatomic distances. In the region of the spectrum containing crosspeaks between the sugar H1'/cytosine H5 and the H2/H6/H8 aromatic protons, as well as in the region containing crosspeaks between the sugar H2'/H2" and the H2/H6/H8 aromatic protons, the connectivity is interrupted around the 8oxoG lesion base itself because its H8 aromatic proton has been replaced by a keto group. On the complementary strand, the walk continues past the lesion uninterrupted (Supp. Fig. 3,4), which confirms that the 8oxoG lesion duplex forms a fully annealed and stable B-form helix. The imino-imino walk from base to base down the center of the helix is also not interrupted by the presence of the lesion, indicating that base pairing is intact along the entire helix (Fig. 3A,B).

Because the 8oxoG lesion does not perturb the global B-form conformation, it is more informative to directly compare the parent and lesion duplexes. By assigning peaks in both the parent duplex and the 8oxoG duplex spectra and overlaying the two, we could evaluate the overall effect of the lesion on duplex structure both in specific location and magnitude. Critically, the NOESY spectra for the parent and 8oxoG lesion duplex are quite similar in every region in terms of peak shape, intensity, and chemical shift (for example, Supp. Fig 5). A careful measurement of chemical shift differences between lesion and parent duplex spectra shows that, not surprisingly, the most marked differences between parent and lesion duplex occur in the base and sugar protons immediately flanking the 8oxoG lesion and in the cytosine Watson-Crick partner (Supp. Table 4). To facilitate visualization of the locations and magnitudes of observed changes, we constructed a simple model of parent duplex **1–2** using Nucleic Acid Builder and color-coded the chemical shift differences observed in the lesion duplex **1oxo-2** (Fig. 4). The A_7 and A_9 aromatic H8 protons, the C_{23} amino protons, the T_{24} imino proton, and the A_7 and G_8 sugar proton resonances show the largest differences between lesion duplex and parent duplex; the G_8 H1’ proton disappears altogether. Overall, modest but measurable differences in chemical shift were observed in the 2–3 base pairs flanking the lesion, particularly on the lesion strand. The chemical shifts of the nucleotides more than 3 base pairs away from the 8oxoG are not perturbed by the presence of the lesion (within the error of measurement, i.e. <0.02 ppm).

Exploring 8oxoG Lesion Base Pair Stability Using the Exchange Rate of the Guanine N1 and Thymine N3 Imino Protons

We chose this 15-mer duplex from among a group of duplex sequences based upon the generally good dispersion of the imino proton resonances in both parent and 8oxoG lesion duplexes, as measured in phosphate buffer at pH 7.5 and 8°C. Assignment of the 2D NOESY spectra allowed us to unequivocally identify these peaks in the 1D ^{1}H NMR spectrum (Fig. 5). As is generally the case, the thymine N3 imino resonances are found slightly downfield from the guanine N1 imino resonances. The 8oxoG_8 N1 imino peak is

shifted downfield compared to its parent G_8 by 0.28 ppm, and the T_{24} imino, which flanks 8oxoG_8's cytosine complement, shifts upfield by 0.09 ppm. However, the remainder of the imino proton resonances change very little in going from parent to lesion duplex. The peaks corresponding to the terminal guanines G_{16} and G_{30} are short and broad due to fraying of the DNA duplex, but the single large peak corresponding to both G_{29} and G_{14} (the penultimate guanines located 1 bp in from the ends of the duplex) is sharp. Notably, the 8oxoG_8 N1 imino proton resonance is not broadened and its amplitude is equivalent to that of the other guanines, indicating that it is base paired and stacked much like a normal guanine. In contrast, the 8oxoG_8 N7 imino proton resonance is significantly smaller and broader, as expected for an imino proton facing outwards into the major groove (inset, Fig. 5B).

With the imino proton assignments in hand, we set out to measure the exchange rate of these protons with water as a handle for exploring the stability and dynamics of the 8oxoG-C base pair and its neighbors in double-helical DNA as described by Guéron (36, 48), Russu (49, 50), Stivers (22, 23), and their respective coworkers. Magnetization transfer from water protons is used to measure the exchange rate of DNA imino protons because this rate is too fast to measure by direct titration of deuterium oxide in real time. Plots of the amplitude of each imino peak as a function of mixing time show that protons on the internal bases (i.e. G_6, G_{12}, or G_{21}) exchange less with the solvent than those near the end (the peak corresponding to the penultimate bases G_{29}/G_{14}, and the terminal peak labeled "term," corresponding to either G_{16} or G_{30}) (Fig. 6). Interestingly, the curve corresponding to the 8oxoG_8 imino proton is similar to that of the other internal guanine protons. Each curve was fitted to Eqn. 4 to estimate an exchange rate k_{ex} for each proton in the duplex. To deconvolute overlapping peaks, the values of k_{ex} were further refined by a multiparameter fit of the whole set of spectra at all time points as described in the methods section (Supp. Tables 5,6 and Supp. Fig. 6).

Unfortunately, these imino proton exchange rates do not directly reveal the rate or equilibrium constant of base pair opening, because the base pair may open and close many times without exchanging a proton with the solution. Thus the values for k_{ex} determined in sodium phosphate buffer dramatically underestimate the rate of base pair opening. To increase the rate of imino proton exchange with solvent, we titrated in a glycine base catalyst and determined the exchange rate of each imino proton at each concentration point as described in the previous paragraphs. The exchange rates determined for each imino proton on the parent and 8oxoG lesion duplex are shown in histogram form for three concentrations across the range tested: 5 mM, 100 mM, and 1000 mM glycine (Fig 7). Note that T_{24}, T_{28}, and T_{11} are not included in the histogram because these peaks overlap substantially in the 8oxoG lesion duplex 1D spectrum. The peaks for the penultimate bases G_{29} and G_{14} also overlap completely, but because of their similar location in the sequence (i.e. with a terminal GC base pair to their 3' side) and similar flanking sequence (a thymine to the 5' side), we assumed for the purposes of calculation that they behaved identically.

At 5 mM total glycine (12.5 μM active base), the lowest concentration of base catalyst, the terminal proton (G_{16} or G_{30}) and the 8oxoG outward-facing N7 have the largest exchange rates on the order of ~100 s^{-1} (Fig. 7A,B). The k_{ex} of the other imino protons is significantly smaller, on the order of 2 s^{-1}, and is similar between parent and lesion duplex (blue vs. red, respectively). Notably, the rate of exchange of the 8oxoG_8 base-pairing N1 proton is only slightly faster than the corresponding proton in the parent duplex (red arrow). By 100 mM total glycine (250 μM base catalyst), the peaks corresponding to the terminal base imino proton and 8oxoG_8 N7 proton have become too small and broad to measure, consistent with fast exchange of protons not involved in stable, long-lived hydrogen bonds. The exchange rate of the penultimate residues G_{29}/G_{14} increases to ~7 s^{-1}, but k_{ex} of the other imino

protons increases only subtly (Fig. 7C). By 1000 mM total glycine (2.5 mM base catalyst), the exchange rate of the penultimate residues G_{29}/G_{14} increases to > 20 s^{-1}, but k_{ex} of the other imino protons still hovers around 3 s^{-1} (Fig. 7D). Even at this heightened glycine concentration, the exchange rate of the 8oxoG N1 proton is only slightly higher than that of the parental G_8 proton.

To determine whether the 8oxoG-C base pair is destabilized and open to solvent more than an unmodified guanine, we plotted these exchange rates as a function of glycine catalyst concentration (Fig. 8) and fit the resulting lines to Eqn. 8 to obtain the apparent equilibrium constant for base pair opening, αK_{op}. It is clear from Eqn. 8 that the slopes of the lines in Fig. 8 are proportional to αK_{op} and k_B (a constant describing the bimolecular collision rate, calculated as described in the Methods section), while the intercept is equal to the product of αK_{op} and k_{int}, the rate of intrinsic catalysis by bases in the DNA. Because of their steep slope, G_{29} and G_{14} clearly have a larger equilibrium constant than the other base pairs, and therefore these base pairs must be open to solvent more than the others consistent with their location adjacent to the ends of the duplex. The lines for the remaining bases have a shallow slope consistent with apparent equilibrium constants on the order of 10^{-6} or smaller. Values of αK_{op} and k_{int} determined from fits to these data are shown in Table 2. Most importantly, within the error established here the equilibrium constant for the opening of the $8oxoG_8$ base is not larger than its matched guanine G_8 in the parent strand nor other similar guanines in either duplex.

To determine directly the *rate* of base pair opening (k_{op}) of the $8oxoG_8$ base and the other DNA bases, we would have to increase the concentration of glycine beyond 2.5 mM glycine base (1000 mM total glycine). However, it is clear that even below 1000 mM, glycine modifies the structure of the DNA. At 100 mM glycine the melting temperature behavior of the duplex changes, with the T_m shifting ~1°C lower (Fig. 9A). This decrease in melting temperature contrasts directly with ammonia, another exchange catalyst commonly used in these types of experiments, which significantly stabilizes the DNA at 100 mM concentration, increasing the T_m by ~ 4°C. We directly observed this change in DNA structure in the NMR spectra as well. With increasing glycine concentration, all of the imino peaks move gradually upfield. The guanine peaks generally retain their chemical shifts relative to one another, but the thymine peaks move significantly relative to one another, changing the pattern of overlapping and distinct peaks (Fig. 9B). These shifts indicate that some changes in the electronic environment of the bases are occurring with increasing glycine, and that these changes are not evenly distributed across the duplex. Thus the values of αK_{op} and k_{int} reported above are only based upon data obtained at 600 mM and below, and no efforts were made to continue the titration beyond 1000 mM glycine.

Direct measurement of the rate of 8oxoG-C base pair opening and closing proved to be impossible with the glycine catalyst at pH 7.5. Glycine is a stronger base than ammonia and therefore in theory a better catalyst; the zwitterionic inactive form might be expected to bind the DNA less strongly than ammonium, and indeed the duplex melting temperature shows a smaller perturbation at 100 mM concentration by glycine than ammonia (Fig. 9A). Even so, far too little of the catalyst is active at this pH to efficiently abstract protons from the DNA, and the size and negative charge of the active catalyst form restrict its ability to access the imino protons effectively.

Discussion

The 8-oxoguanine lesion is believed to be formed at the staggering rate of thousands per mammalian cell per day, and if left unrepaired, it can have dire effects upon the cell and the organism (1, 51). Over the last two decades several groups have explored the structure and

thermodynamic stability of 8-oxoguanine and have observed that DNA containing 8oxoG tends to be similar to unmodified DNA(10, 11, 15, 52). This apparent similarity raises the question of how it can be detected and repaired at all. Here we brought to bear a variety of different types of experiments on the same nonpalindromic 15-mer duplex containing a single centrally-located 8oxoG lesion, specifically looking at base pair opening as an unstudied and potentially critical factor in discrimination between lesion and normal guanine.

Structural and Thermodynamic Effects of the 8oxoG Lesion on DNA

Using circular dichroism spectropolarimetry, we confirmed that our 8oxoG duplex is B-form and globally unperturbed by the lesion, as seen previously with 8oxoG in other sequences (15, 52, 53). The broad band around 275 nm that is a composite of $\pi\rightarrow\pi^*$ and $n\rightarrow\pi^*$ electronic transitions on the DNA bases changes slightly upon addition of the lesion, in this case decreasing slightly but in some cases increasing slightly (Fig. 1A) (15, 44, 52, 53). The shape and intensity of this band have been described as reflecting π stacking, indirectly reporting about changes in helical twist and base pair tilt (54). However, the electron distribution and dipole moment of 8oxoG are quite different than that of unmodified guanine (7, 8). Considering that the molar extinction coefficient for the UV absorption of 8oxoG at 260 nm is less than that of guanine by ~6300 M^{-1} cm^{-1}, it is not unreasonable to hypothesize that the changes we see in the CD spectrum of the lesion duplex are largely due to localized electronic changes on the lesion base rather than larger structural ones.

This picture of a structurally-conserved duplex with electronic differences localized to the lesion site is supported by comparison of parent duplex **1–2** and lesion duplex **1oxo-2** NOESY spectra (Fig. 3; Supp. Fig. 3–5). The imino-imino NOE walk is thoroughly conserved past the lesion base, showing that base pairing is stable at the lesion. The H1'-aromatic base walk and H2'/H2"-aromatic base walk are also thoroughly conserved on the complementary strand, indicative of a B-form helix. As expected, the H8 aromatic proton on the lesion strand is missing at the 8oxoG lesion site, but a thorough search for all possible crosspeaks shows the $8oxoG_8$ H1' sugar proton to be missing completely from the spectrum also. It seems most likely that the H1' resonance has shifted from 5.459 ppm in the parent to ~ 4.7 ppm in the lesion strand (disappearing under the residual water resonance), reflecting the dramatically different electronic environment it experiences directly 3' to the 8-oxo group (Fig. 4C). The neighboring $8oxoG_8$ H2" proton resonance moves by more than 0.5 ppm downfield, so by comparison a 0.67 upfield change in the H1' chemical shift seems logical in both magnitude and direction. The H1' proton is more shielded in the lesion duplex than the parent, but the H2" proton is more deshielded in the lesion duplex. Because of their slightly different positions under the lesion base, each proton experiences a unique, and clearly opposite, change in its electronic environment due to the 8oxoG base dipole (10). However, without either the aromatic or the H1' resonance it is difficult to establish whether the $8oxoG_8$ sugar pucker is different from that of the parent due to crowding from the extra carbonyl oxygen at the 8 position. Early structural data are inconclusive on this point, but recent crystallographic evidence points to a C2'-*endo* configuration on the 8oxoG nucleotide's sugar in a different duplex sequence (12).

A quantitative comparison of proton chemical shifts throughout the duplex reveals that changes are highly localized to the bases and sugars closest to the lesion site, consistent with the only other published NOESY spectrum of DNA containing 8oxoG-C base pairs (Fig. 4) (10). Because our oligonucleotide duplex is 15 bp long with seven normal base pairs on either side of the lesion, we can uniquely demonstrate that the effects of the lesion drop off steeply with distance. Indeed, no difference in chemical shift is seen for protons on nucleotides more than 3 bp away from the lesion. Protons on the complementary strand are significantly less affected by the lesion, with the exception of the C_{23} N4 amino proton and

the T_{24} imino proton. Because the C_{23} N4 amino proton is directly hydrogen-bonded to the 8oxoG lesion base, it should be particularly sensitive to electronic changes to that guanine. Similarly, the T_{24} imino proton is stacked immediately below the 8oxoG base. In contrast the C_{23} C5 and C6 aromatic protons, which point outward toward the major groove and away from the 8oxoG lesion base, display much smaller changes in chemical shift, supporting the idea that 8oxoG's primary effect on duplex DNA structure could be electronic rather than steric. Such electronic effects may serve as a distinctive repair signal in the absence of large structural distortions (55, 56).

Having seen that the structure of this nonpalindromic 15-mer duplex containing an 8oxoG-C base pair is essentially the same as its control duplex in terms of overall shape and conformation, we also probed the thermodynamic stability of the duplexes. A van't Hoff analysis of UV melting revealed that in this relatively long duplex, the 8oxoG lesion has almost no effect on the overall double strand-single strand equilibrium (Fig. 1BC), consistent with 8oxoG's effects measured by other groups using shorter duplexes and/or different flanking sequences (15, 52, 53). Similarly, the mismatch-sensitive photocleavage agent $Rh(bpy)_2(chrysi)^{3+}$ was unable to detect the presence of 8oxoG in this 15-mer duplex. The latter result is particularly interesting because the $Rh(bpy)_2(chrysi)^{3+}$ has been shown to detect some mismatch sites much more effectively than others, reflecting primarily local thermodynamic stability and also steric or kinetic factors. This differential cleavage allows us to roughly rank the plasticity of the 8oxoG-C site within a range of noncanonical sites (46, 47). The more stable mismatches that can stack well and form some hydrogen bonds, such as a G-A mismatch, are poorly bound and cleaved by $Rh(bpy)_2(chrysi)^{3+}$, whereas open, unstable mismatches such as CC are detected robustly. Within this context, the 8oxoG-C pair seems to be less open and accessible than a pyrimidine-pyrimidine mismatch. Furthermore, the fact that the 8oxoG site was not bound and cleaved efficiently, even when we mispaired it with adenine, points to the fact that the double helix is *locally* stable at the site of the 8oxoG and not just *globally* stable as revealed by the van't Hoff analysis.

Effect of the 8oxoG Lesion on Base Pair Opening

To discover whether the 8oxoG lesion has a kinetic or dynamic effect on the DNA helix, we set out to determine the rate of base pair opening for all of the bases in the lesion and control duplex. Fortunately, unlike some base lesions the 8oxoG lesion retains the imino proton of its unmodified precursor, giving us the handle to examine base pair opening. Even between 5–100 mM glycine, it is clear that the rate of exchange of the 8oxoG imino proton is similar to most of the internal guanines but is distinctly different from the terminal bases, the penultimate bases G_{29}/G_{14}, and the 8oxoG N7 imino proton (Fig. 7). The 8oxoG N7 proton provides a fascinating internal control given that it is located on the same lesion base only a few Ångstroms away from the N1. The $8oxoG_8$ N7 imino proton exchanges much more quickly than the N1 imino proton even though it is much slower to tautomerize and its pK_a is calculated to be almost four pH units higher (7, 9). The fact that the N7 proton exchanges so rapidly with the solution confirms that it faces outward into the major groove rather than toward the complementary cytosine, in direct contrast to the N1. The terminal bases also exchange very quickly because they need not strictly open to the solution to exchange their imino proton; solvent molecules can approach the face of the bases directly even when the bases are stacked and base-paired, and as a result they can abstract protons with facility. The penultimate bases G_{29}/G_{14} provide an interesting third comparison. As guanines they are reasonable controls for the 8oxoG sterically and electronically, and they do lack the direct steric access issues of the terminal bases. However, even at 8°C the ends of the DNA duplex fray, and the base pairing face becomes accessible to the solution. These penultimate base pairs open slowly and infrequently enough to have sharp NMR resonances even at the highest glycine concentrations, but they are clearly more mobile and/or accessible to

solution than the internal bases. The 8oxoG exchange rates are distinct from all of these, being similar to but slightly larger than the corresponding guanine G_8 in the parent duplex (Fig. 7; Supp. Fig. 7). Though this slight difference might appear to indicate a difference in opening rate or thermodynamics, it must be noted that the 8oxoG imino proton has a pK_a around 0.7 pH units lower than normal guanine, meaning that it is more acidic and therefore easier to deprotonate (7). When the difference in pK_a is taken into account (the k_B term in eqn. 8), the apparent equilibrium constant for base pair opening of the 8oxoG base is essentially the same as that of the corresponding parental base G_8, and the other internal guanine bases (Table 2). That the intrinsic rate of proton exchange from the 8oxoG base is slightly larger than the exchange from the parental control base is probably due to the same pK_a effect.

At the glycine concentrations measured, abstraction of most of the imino protons is quite inefficient and the slopes of the lines in figure 8 are shallow, so as a result the errors in our estimates of guanine αK_{op} values are on the order of 20–30%. Thus it is quite possible that the apparent equilibrium constant for opening of the 8oxoG-C is *slightly* larger than that of a control GC pair. Nonetheless, we can exclude the possibility of 8oxoG's αK_{op} being much larger than G_8 based on the upper bound provided by the penultimate bases G_{29}/G_{14}, which have equilibrium constants ten times larger but which also exchange at a rate that is clearly distinct from 8oxoG. Note that apparent equilibrium constants on the order of 10^{-6} agree with those measured by this method in other short DNA duplexes (22, 36). Depending on the value of α, this equilibrium constant is equivalent to a free energy cost for breaking a base pair between 6–7 kcal/mol, consistent with calculated energy costs for breaking G-C and 8oxoG-C base pairs (24, 41, 57).

Because the apparent equilibrium constant αK_{op} is the same for 8oxoG as for the other guanine bases, we can say that the overall fraction of time that the 8oxoG-C base pair spends open to solution is the same as the amount of time that a G-C base pair spends open (i.e. one millionth). However, we could not directly determine the rates of base pair opening k_{op} and closing k_{cl} because imino exchange was too weakly catalyzed over this range of glycine concentrations. As a result, we cannot exclude the possibility that the *rate* of 8oxoG-C base pair opening is faster than that of G-C. If that were the case, any increases in the rate of opening would have to be matched by equivalent increases in the rate of base pair closing since αK_{op} is equal to the ratio of the opening and closing rates (Eqn. 6). Conversely, an open 8oxoG-C base pair might conceivably close more slowly than a G-C base pair, but then it would also have to open more slowly. Either might facilitate detection and repair, the former by decreasing the activation energy of base pair opening, and the latter by prolonging the lifetime of the extrahelical state (Fig. 10).

It is important to remember that this imino proton exchange model assumes a two state, open-or-closed model of base pair opening, when in fact that is unlikely to be the case (36). Molecular dynamics simulations suggest that the purine base, the pyrimidine base, or both might rotate out of the helix to open to solvent, and opening may occur through either the major or minor grooves depending on the steric and energetic limitations (57). “Opening” itself is a slightly murky term, since the bases do not have to swing out by 180° or even 90° in order to make possible hydrogen exchange between solvent protons and base imino protons (58, 59). Nevertheless, breaking the hydrogen bonds and unstacking at least one base from the hydrophobic core of the helix, i.e. the energetic barrier measured by proton exchange measurements, is not only the initial step but also likely the largest energetic contributor to any opening process. The free energy associated with this critical step appears to be the same for the 8oxoG-C base pair as for a GC base pair.

DNA can be considered a dynamic molecule over many time scales, ranging from short-range vibrational and electronic fluctuations occurring at subpicosecond time scales, to bending and twisting motions occurring on the picosecond to nanosecond time scales, to base pair opening on the microsecond to millisecond time scales, to a variety of large-scale, activated, or cooperative processes occurring at longer times (48, 60, 61). Given the critical role of base pair flipping in glycosylase mechanisms, we chose to focus on changes in spontaneous base pair opening dynamics around the 8oxoG lesion. However, the bending, curvature, or dynamic movement of 8oxoG-containing DNA on other time scales or other size scales may yet prove to be more distinctive than the base pair opening dynamics (16, 62).

Enzymatic detection of 8oxoG-C base pairs may exploit other subtle differences between lesion and normal base pairs. Subtle changes to water molecule and cation binding around an 8oxoG-C base pair, with corresponding small changes to sugar-phosphate backbone angles, have been predicted computationally (18) and demonstrated experimentally using calorimetric methods and γ ray footprinting (52, 63).

Biological Implications for 8-oxoguanine Repair

Extensive work on the mechanisms of DNA base excision repair glycosylases have demonstrated that they bind the DNA nonspecifically and quickly scan the genome for lesions by sliding along the DNA for short periods interspersed with hopping (64). When they find a base lesion, they bind it extrahelically and cleave it at the glycosidic bond (65). Though the chemistry of the cleavage mechanisms is well understood, the initial enzyme-lesion encounter and recognition events remain an active area of research (20, 66). The evidence presented here that the equilibrium constant for 8oxoG-C base pair opening is the same as that of a normal G-C base pair provides a critical piece of information about the parameters for recognition and extrusion of this lesion. Since 8-oxoguanine remains securely buried in the helix the vast majority of the time, it seems likely that repair enzymes may have to exploit yet-unmeasured differences in opening and closing rates, sense electronic differences between the oxidized and normal base, detect new bending modes or changes to water molecule binding, or actively perturb the DNA in order to detect the lesion.

Conclusions

Here we have shown that a 15-mer DNA duplex containing an 8-oxoG-C base pair is both globally and locally almost indistinguishable from a control normal duplex. Not only is the lesion duplex B-form and similar in overall thermodynamic stability to the control duplex as shown by CD spectropolarimetry and van't Hoff analysis, but the immediate vicinity of the lesion is also well-conserved. 2D NOESY spectra reveal that differences between the duplexes are localized to the lesion, with the flanking bases beyond the immediate two base neighbors and most of the complementary strand being completely unaffected by the lesion. The base-mismatch agent $Rh(bpy)_2chrysi^{3+}$ shows no clear preference for binding the lesion site over other Watson-Crick sites. Most notably, NMR imino exchange measurements indicate that the intrahelical stability of the 8-oxoguanine–cytosine base pair is the same as that of normal GC base pairs. When taken together, this group of structural and thermodynamic measurements performed side-by-side on the same non-palindromic 15-mer duplex confirm that the 8oxoG lesion is indeed well-hidden in a B-form DNA duplex, leaving open continued speculation about how this common pro-mutagenic lesion is detected and repaired.

Supplementary Material

Refer to Web version on PubMed Central for supplementary material.

Abbreviations

8oxoG	8-oxo-7,8-dihydro-2'-deoxyguanosine or 8-oxoguanine
NMR	nuclear magnetic resonance spectroscopy
NOESY	Nuclear Overhauser effect spectroscopy
BER	Base excision repair
PAGE	polyacrylamide gel electrophoresis
CD	circular dichroism spectropolarimetry
HPLC	high performance liquid chromatography
$Rh(bpy)_2(chrysi)^{3+}$	bis(2,2'-bipyridine)(5,6-chrysenequinone diimine)rhodium(III)
k_{ex}	rate of imino proton exchange
k_{op}	rate of base pair opening
αK_{op}	apparent equilibrium constant for base pair opening

Acknowledgments

MEN would like to extend her deepest thanks to Professor Gregory Verdine and his laboratory group for generously providing space for and encouragement of this project. We would also like to thank Dr. Jean-Christophe Hus for sharing with us his Python scripts for NMR spectral processing in NMR Pipe, Ms. Elisa Frankel for her expertise with DNA melting experiments, Ms. Sara Barnes for gel electrophoresis support, Dr. Mandy Blackburn in the Gierasch lab at UMass for help with the CD, and Dr. Jacqueline Barton for the gift of $Rh(bpy)_2chrysi^{3+}$.

References

1. Friedberg, EC.; Walker, GC.; Siede, W.; Wood, RD.; Schultz, RA.; Ellenberger, T. DNA Repair and Mutagenesis. 2nd ed. Washington, D.C.: ASM Press; 2006.
2. Dedon PC. Oxidation and deamination of DNA by endogenous sources. Current Cancer Research: Chemical Carcinogenesis. 2011:209–225.
3. Burrows CJ, Muller JG. Oxidative nucleobase modifications leading to strand scission. Chem. Rev. 1998; 98:1109–1151. [PubMed: 11848927]
4. Steenken S, Jovanovic S. How easily oxidizable is DNA? One-electron reduction potentials of adenosine and guanosine radicals in aqueous solution. J. Am. Chem. Soc. 1997; 119:617–618.
5. Shibutani S, Takeshita M, Grollman AP. Insertion of specfic bases during DNA synthesis past the oxidation-damaged base 8-oxodG. Nature. 1991; 349:431–434. [PubMed: 1992344]
6. Hsu GW, Ober M, Carell T, Beese LS. Error-prone replication of oxidatively damaged DNA by a high-fidelity DNA polymerase. Nature. 2004; 431:217–221. [PubMed: 15322558]
7. Jang YH, Goddard WA III, Noyes KT, Sowers L, Hwang S, Chung DS. First principles calculations of the tautomers and pK_a values of 8-oxoguanine: implications for mutagenicity and repair. Chem. Res. Toxicol. 2002; 15:1023–1035. [PubMed: 12184786]
8. Banerjee A, Yang W, Karplus M, Verdine GL. Structure of a repair enzyme interrogating undamaged DNA elucidates recognition of damaged DNA. Nature. 2005; 434:612–618. [PubMed: 15800616]
9. Cho BP, Kadlubar FF, Culp S, Evans F. ^{15}N nuclear magnetic resonance studies on the tautomerism of 8-hydroxy-2'-deoxyguanosine, 8-hydroxyguanine, and other C8-subsituted guanine nucleosides. Chem. Res. Toxicol. 1990; 3:445–452. [PubMed: 2133096]
10. Oda Y, Uesugi S, Ikehara M, Nishimura S, Kawase Y, Ishikawa H, Inoue H, Ohtsuka E. NMR studies of a DNA containing 8-hydroxydeoxyguanosine. Nucleic Acids Res. 1991; 19:1407–1412. [PubMed: 2027747]

11. Lipscomb LA, Peek ME, Morningstar ML, Verghis SM, Miller EM, Rich A, Essigmann J, Williams LD. X-ray structure of a DNA decamer containing 7,8-dihydro-8-oxoguanine. Proc. Natl. Acad. Sci. USA. 1995; 92:719–723. [PubMed: 7846041]
12. Bowman BR, Lee S, Wang S, Verdine GL. Structure of the *E. coli* DNA glycosylase AlkA bound to the ends of duplex DNA: A system for the structure determination of lesion-containing DNA. Structure. 2008; 16:1166–1174. [PubMed: 18682218]
13. McAuley-Hecht K, Leonard GA, Gibson NJ, Thomson JB, Watson WP, Hunter WN, Brown T. Crystal structure of a DNA duplex containing 8-hydroxydeoxyguanine-adenine base pairs. Biochemistry. 1994; 33:10266–10270. [PubMed: 8068665]
14. Kouchakdjian M, Bodepudi V, Shibutani S, Eisenberg M, Johnson F, Grollman AP, Patel DJ. NMR structural studies of the ionizing radiation adduct 7-hydro-8-oxodeoxyguanosine (8-oxo-7H-dG) opposite deoxyadenosine in a DNA duplex. 8-Oxo-7H-dG (*syn*)*dA (*anti*) alignment at lesion site. Biochemistry. 1991; 30:1403–1412. [PubMed: 1991121]
15. Plum GE, Grollman AP, Johnson F, Breslauer KJ. Influence of the oxidatively damaged adduct 8-oxodeoxyguanosine on the conformation, energetics, and thermodynamic stability of a DNA duplex. Biochemistry. 1992; 34:16148–16160. [PubMed: 8519772]
16. Miller JH, Fan-Chiang C-C, Straatsma TP, Kennedy MA. 8-oxoguanine enhances bending of DNA that favors binding to glycosylases. J. Am. Chem. Soc. 2003; 125:6331–6336. [PubMed: 12785867]
17. Ishida H. Molecular dynamics simulation of 7,8-dihydro-8-oxoguanine DNA. J. Biomol. Struct. Dyn. 2002; 19:839–851. [PubMed: 11922839]
18. Naômé A, Schyman P, Laaksonen A, Vercauteren DP. Molecular dynamics simulation of 8-oxoguanine containing DNA fragments reveals altered hydration and ion binding patterns. J. Phys. Chem. B. 2010; 114:4789–4801. [PubMed: 20307074]
19. Cheng X, Kelso C, Hornak V, de los Santos C, Grollman AP, Simmerling C. Dynamic behavior of DNA base pairs containing 8-oxoguanine. J. Am. Chem. Soc. 2005; 127:13906–13918. [PubMed: 16201812]
20. David SS, O'Shea VL, Kundu S. Base-excision repair of oxidative DNA damage. Nature. 2007; 447:941–950. [PubMed: 17581577]
21. Verdine GL, Bruner SD. How do DNA repair proteins locate damaged bases in the genome? Chem. & Biol. 1997; 4:329–334. [PubMed: 9195879]
22. Cao C, Jiang Y, Stivers J, Song F. Dynamic opening of DNA during the enzymatic search for a damaged base. Nat. Struct. Mol. Biol. 2004; 11:1230–1236. [PubMed: 15558051]
23. Parker J, Bianchet M, Krosky D, Friedman JI, Amzel L, Stivers J. Enzymatic capture of an extrahelical thymine in the search for uracil in DNA. Nature. 2007; 449:433–437. [PubMed: 17704764]
24. Qi Y, Spong MC, Nam K, Banerjee A, Jiralerspong S, Karplus M, Verdine GL. Encounter and extrusion of an intrahelical lesion by a DNA repair enzyme. Nature. 2009; 462:762–766. [PubMed: 20010681]
25. Ivanov V, Krylov D. A-DNA in solution as studied by diverse approaches. Meth. Enzymol. 1992; 211:111–127. [PubMed: 1406304]
26. Sambrook, J.; Russell, DW. Molecular cloning: A laboratory manual. 3rd ed. Cold Spring Harbor, New York: Cold Spring Harbor Laboratory Press; 2001.
27. Liu M, Mao X, He C, Huang H, Nicholson JK, Lindon JC. Improved WATERGATE Pulse Sequences for Solvent Suppression in NMR. J. Magn. Reson. 1998; 132:125–129.
28. Jeener J, Meier BH, Bachmann P, Ernst RR. Investigation of exchange processes by two-dimensional NMR spectroscopy. J. Chem. Phys. 1979; 71:4546–4653.
29. Macura S, Ernst RR. Elucidation of cross relaxation in liquids by two-dimensional N.M.R. spectroscopy. Mol. Phys. 1980; 41:95–117.
30. Delaglio F, Grzesiek S, Vuister GW, Zhu G, Pfeifer J, Bax A. NMRPipe: a multidimensional spectral processing system based on UNIX pipes. J. Biomol. NMR. 1995; 6:277–293. [PubMed: 8520220]
31. Goddard, TD.; Kneller, DG. Sparky 3. San Francisco: University of California;

32. Wemmer, D. Structure and Dynamics by NMR. In: Bloomfield, V.; Crothers, DM.; Tinoco, I., editors. Nucleic Acids: Structures, Properties, and Functions. Sausalito, CA: University Science Books; 2000.
33. Hare DR, Wemmer D, Chou S-H, Drobny G. Assignment of the non-exchangeable proton resonances of d(CGCGAATTCGCG) using two-dimensional nuclear magnetic resonance methods. J. Mol. Biol. 1983; 171:319–336. [PubMed: 6317867]
34. Scheek RM, Russo N, Boelens R, Kaptein R, van Boom JH. Sequential resonance assignments in DNA proton NMR spectra by two-dimensional NOE spectroscopy. J. Am. Chem. Soc. 1983; 105:2914–2916.
35. Macke, TJ.; Case, DA. Modeling unusual nucleic acid structures. In: Leontis, NB.; SantaLucia, J., editors. Molecular Modeling of Nucleic Acids. Washington, D.C.: American Chemical Society; 1998. p. 379-393.
36. Guéron M, Leroy JL. Studies of base pair kinetics by NMR measurement of proton exchange. Meth. Enzymol. 1995; 261:383–413. [PubMed: 8569504]
37. Plateau P, Guéron M. Exchangeable proton NMR without base-line distortion, using new strong-pulse sequences. J. Am. Chem. Soc. 1982; 104:7310–7311.
38. Morris GA, Freeman R. Selective excitation in Fourier transform Nuclear Magnetic Resonance. J. Magn. Reson. 1978; 29:433–462.
39. Sikorski WH, Sanders AW, Reich HJ. Tris(trimethylsilyl)methane as an internal ^{13}C NMR chemical shift thermometer. Magn. Reson. Chem. 1998; 36:S118–S124.
40. Raiford D, Fisk C, Becker ED. Calibration of methanol and ethylene glycol nuclear magnetic resonance thermometers. Anal. Chem. 1979; 51:2050–2051.
41. Guéron, M.; Charretier, E.; Hagerhorst, J.; Kochoyan, M.; Leroy, JL.; Moraillon, A. Applications of imino proton exchange to nucleic acid kinetics and structures. In: Sarma, RH.; Sarma, MH., editors. Structure and Methods Volume 3: DNA & RNA. Proceedings of the Sixth Conversation in the Discipline of Biomolecular Stereodynamics Held at the State University of New York at Albany, June 6–10, 1989. Schenectady, N.Y.: Adenine Press; 1990.
42. Every AE, Russu IM. Influence of magnesium ions on spontaneous opening of DNA base pairs. J. Phys. Chem. B. 2008; 112:7689–7695. [PubMed: 18512983]
43. Gray DM, Ratliff RL, Vaughan MR. Circular dichroism spectroscopy of DNA. Meth. Enzymol. 1992; 211:389–406. [PubMed: 1406317]
44. Bush, CA. Basic Principles in Nucleic Acid Chemistry. New York: Academic Press; 1974. Ultraviolet spectroscopy, circular dichroism, and optical rotatory dispersion.
45. Kypr J, Kejnovska I, Renciuk D, Vorlickova M. Circular dichroism and conformational polymorphism in DNA. Nucleic Acids Res. 2009; 37:1713–1725. [PubMed: 19190094]
46. Jackson BA, Alekseyev VY, Barton JK. A versatile mismatch recognition agent: specific cleavage of a plasmid DNA at a single mispair. Biochemistry. 1999; 38:4655–4662. [PubMed: 10200152]
47. Jackson BJ, Barton JK. Recognition of base mismatches in DNA by 5,6-chrysenequinone diimine complexes of rhodium(III): a proposed mechanism for preferential binding to destabilized regions of the double helix. Biochemistry. 2000; 39:6176–6182. [PubMed: 10821692]
48. Guéron M, Kochoyan M, Leroy JL. A single mode of DNA base-pair opening drives imino proton exchange. Nature. 1987; 328:89–92. [PubMed: 3037381]
49. Every AE, Russu IM. Probing the role of hydrogen bonds in the stability of base pairs in double-helical DNA. Biopolymers. 2007; 87:165–173. [PubMed: 17636510]
50. Folta-Stogniew E, Russu IM. Base-catalysis of imino proton exchange in DNA: effects of catalyst upon DNA structure and dynamics. Biochemistry. 1996; 35:8439–8449. [PubMed: 8679602]
51. Helbock H, Beckman KB, Shigenaga MK, Walter P, Woodall A, Yeo H, Ames B. DNA oxidation matters: the HPLC-electochemical detection assay of 8-oxo-deoxyguanosine and 8-oxo-guanine. Proc. Natl. Acad. Sci. USA. 1998; 95:288–293. [PubMed: 9419368]
52. Barone F, Cellai L, Giordano C, Matzeu M, Mazzei F, Pedone F. Gammaray footprinting and fluorescence polarization anisotropy of a 30-mer synthetic DNA fragment with one 2'-deoxy-7-hydro-8oxoguanosine lesion. Eur. Biophys. J. 2000; 28:621–628. [PubMed: 10663529]

53. Chinyengetere F, Jamieson ER. Impact of the oxidized guanine lesion spiroiminodihydantoin on the conformation and thermodynamic stability of a 15-mer DNA duplex. Biochemistry. 2008; 47:2584–2591. [PubMed: 18281959]
54. Bloomfield, V.; Crothers, D.; Tinoco, I. Nucleic Acids: Structures, Properties, and Functions. Sausalito, California: University Science Books; 2000.
55. Markus TZ, Daube SS, Naaman R, Fleming A, Muller JG, Burrows CJ. Electronic structure of DNA-unique properties of 8-oxoguanosine. J. Am. Chem. Soc. 2008; 131:89–95. [PubMed: 19128174]
56. Yavin E, Stemp EDA, O'Shea V, David SS, Barton JK. Electron trap for DNA-bound repair enzymes: a strategy for DNA-mediated signaling. Proc. Natl. Acad. Sci. USA. 2006; 103:3610–3614. [PubMed: 16505354]
57. Priyakumar UD, MacKerell A. Computational approaches for investigating base flipping in oligonucleotides. Chem. Rev. 2006; 106:489–505. [PubMed: 16464016]
58. Priyakumar UD, MacKerell A. NMR imino proton exchange experiments on duplex DNA primarily monitor the opening of purine bases. J. Am. Chem. Soc. 2005; 128:678–679. [PubMed: 16417331]
59. Spies MA, Schowen RL. The trapping of a spontaneously "flipped out" base from double helical nucleic acids by host-guest complexation with beta-cyclodextrin: the intrinsic base-flipping rate constant for DNA and RNA. J. Am. Chem. Soc. 2002; 124:14049–14053. [PubMed: 12440903]
60. Brauns EB, Madaras ML, Coleman RS, Murphy CJ, Berg M. Complex local dynamics in DNA on the picosecond and nanosecond timescales. Phys. Rev. Lett. 2002; 88:158101–158104. [PubMed: 11955218]
61. Robinson BH, Mailer C, Drobny G. Site-specific dynamics in DNA: experiments. Annu. Rev. Biophys. Biomol. Struct. 1997; 26:629–658. [PubMed: 9241432]
62. Marathias VM, Jerkovic B, Arthanari H, Bolton PH. Flexibility and curvature of duplex DNA containing mismatched sites as a function of temperature. Biochemistry. 2000; 39:153–160. [PubMed: 10625490]
63. Singh S, Szulik M, Ganguly M, Khutsishvilli I, Stone M, Marky L, Gold B. Characterization of DNA with an 8-oxoguanine modification. Nucleic Acids Res. 2011; 39:6789–6801. [PubMed: 21572101]
64. Blainey P, van Oijen AM, Banerjee A, Verdine GL, Xie XS. A base-excision DNA-repair protein finds intrahelical lesion bases by fast sliding in contact with DNA. Proc. Natl. Acad. Sci. USA. 2006; 103:5752–5757. [PubMed: 16585517]
65. Stivers JT, Jiang Y. A mechanistic perspective on the chemistry of DNA repair glycosylases. Chem. Rev. 2003; 103:2729–2759. [PubMed: 12848584]
66. David SS, Williams SD. Chemistry of glycosylases and endonucleases involved in base-excision repair. Chem. Rev. 1998; 98:1221–1261. [PubMed: 11848931]

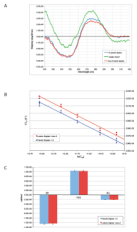

Figure 1. Circular dichroism spectrum and UV melting thermodynamics

(a) CD spectrum of parent duplex **1–2**, lesion duplex **1oxo-2**, and single stranded **1** in sodium phosphate buffer at 10°C. Each strand was present at 8 μM concentration. The shapes of the parent **1–2** and lesion **1oxo-2** duplex spectra (blue and red, respectively) are similar to each other and also consistent with previously published spectra for B-form DNA double helices. (B) van't Hoff plot of the relationship between duplex concentration and melting temperature for parent duplex **1–2** (blue) and lesion duplex **1oxo-2** (red), as described by Eqn. 1. (C) Comparison of the thermodynamic parameters ΔH, −TΔS, and ΔG for formation of the parent (blue) and lesion (red) duplexes at 298 K.

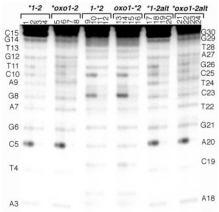

Figure 2. Probing duplex stability with $Rh(bpy)_2(chrysi)^{3+}$

DNA duplexes were incubated with $Rh(bpy)_2(chrysi)^{3+}$ for 10 hours on a visible light box at room temperature to detect destabilized base pairs. The samples were loaded identically in each group of four lanes: Lanes 1, 5, 9, 13, 17, 21: 5 μM chrysi + hν. Lanes 2, 6, 10, 18, 22: 10 μM chrysi + hν. Lanes 3, 7, 11, 15, 19, 23: light control (+ hν but no chrysi). Lane 4, 8, 12, 16, 20, 24: dark control (10 μM chrysi but no hν). Asterisks indicate the strand that is radiolabeled with ^{32}P on its 5' end. The first two groups of lanes compare cleavage in the parent versus the lesion duplex labeled on the primary strand **1** or **1oxo**; the central two groups compare cleavage on duplexes with complementary strand **2** labeled; the last two groups compare cleavage on duplexes with labeled primary strand annealed with an alternative complementary strand containing an adenine at position 23, creating a G_8A_{23} or $oxoG_8A_{23}$ mispair. Sequence of primary strand **1** is shown for comparison at the left side of the gel and of strand **2** on the right side. Note that the darkest bands represent <1% of the total lane, consistent with a low level of binding and cleavage to stable, well-matched DNA duplexes.

3A

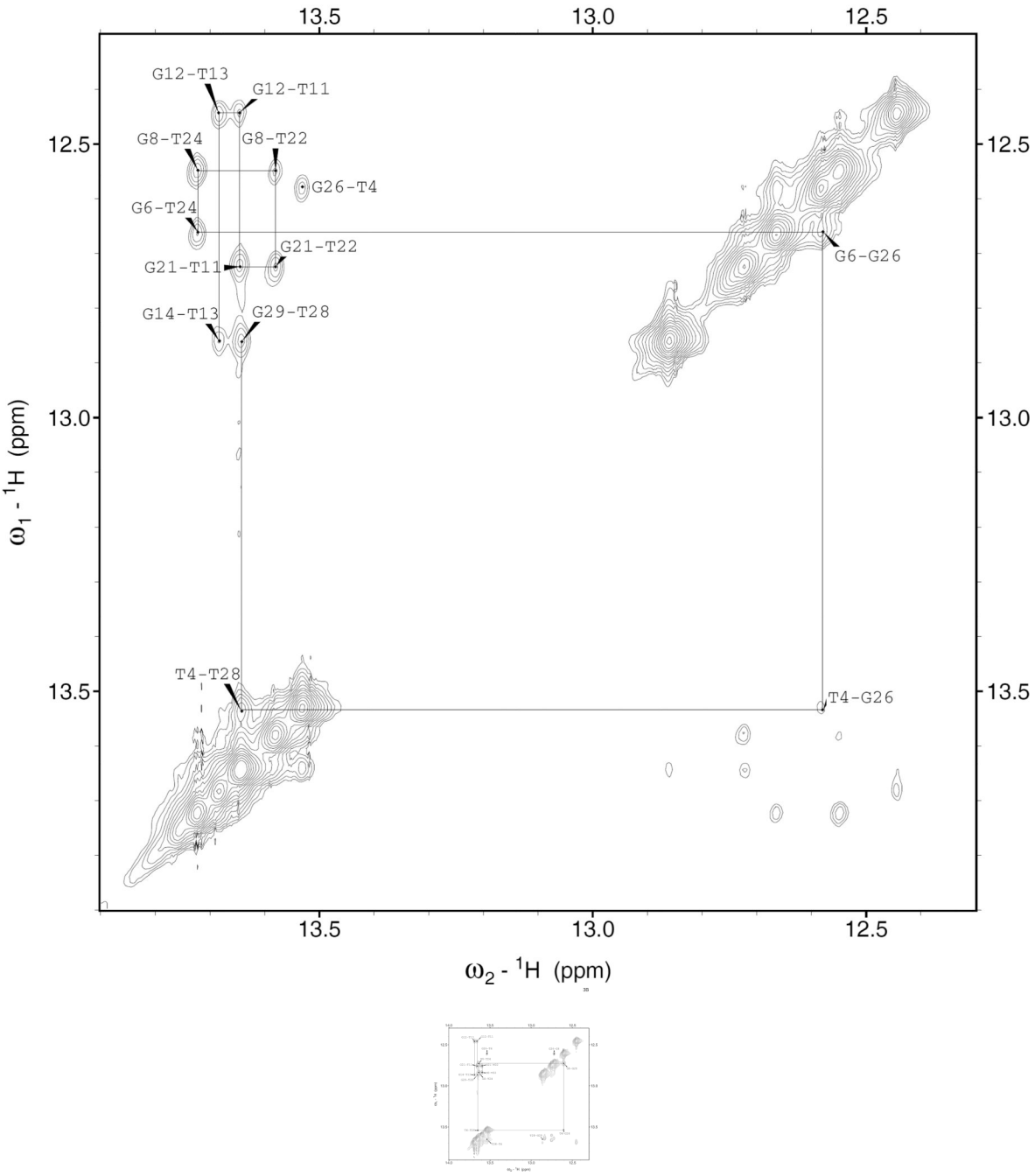

Figure 3. Imino-imino 2D NOESY spectra

These spectra show through-space coupling between guanine N1 and thymine N3 imino protons in neighboring base pairs for the (A) parent duplex **1–2** and (B) 8oxoG lesion duplex

1oxo-2. Crosspeaks in this region were assigned by tracing them consecutively from one end of the helix (G_{29}) to the other (G_{14}), as shown with solid lines. Thymine imino proton resonances are found between 13.5–14 ppm, and guanine imino proton resonances between 12.4–12.9 ppm, so the peaks furthest from the diagonal correspond to G-T and T-G steps; peaks close to the diagonal correspond to G-G or T-T steps. Note that the terminal guanine imino protons exchange too quickly to be seen on the timescale of this NOESY experiment.

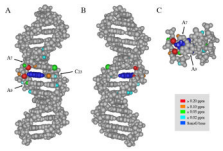

Figure 4. Chemical shift differences between parent and 8oxoG duplex NOESY spectra

Model of duplex **1–2** shown from (A) the major groove, (B) the minor groove, and (C) along the helical axis. Each model is color-coded as indicated in the legend to indicate the magnitude of differences in chemical shift between protons on the parent and lesion duplexes. Guanine 8's base is colored royal blue for clarity; the chemical shift of its imino proton changes significantly due to major electronic differences between guanine and 8oxoG. The default grey color indicates that 1. the chemical shift of the proton did not change (i.e. the protons on the terminal 4 bp at either end of the duplex); 2. the proton chemical shift was not assigned (i.e. the H4' and H5' protons); or 3. the atom is not a hydrogen and/or does not have a hydrogen attached to it that could be assessed by this method (i.e. backbone phosphates, portions of the aromatic bases). The values of all of the chemical shifts included in this figure are tabulated in Supplemental Table 4. Where protons could be measured spectroscopically but are not shown explicitly in this diagram, the carbon or nitrogen to which they are attached has been shaded instead. In panels (A) and (B), the C_1–G_{30} base pair is shown at the top of the duplex. In panel (C), only nucleotides A_7-G_8-A_9 and their complements are shown; the guanine N7 and C8 positions are labeled with white numbers.

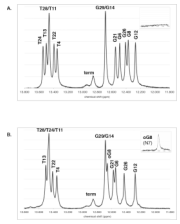

Figure 5. Imino proton region of 1D ^{1}H NMR spectra

(A) **1–2** parent duplex and (B) **1oxo-2** lesion duplex spectra are shown at 8°C and pH 7.5. An additional small, broad proton resonance can be seen around 9.4 ppm in the 8oxoG lesion duplex spectrum in the absence of catalyst, corresponding to the N7 imino proton of the 8oxoG lesion itself (inset). Since guanine does not normally have an N7 imino proton, this peak is missing from the parent duplex. “Term” refers to the terminal G_{16} and G_{30} protons with chemical shifts around 12.9 ppm.

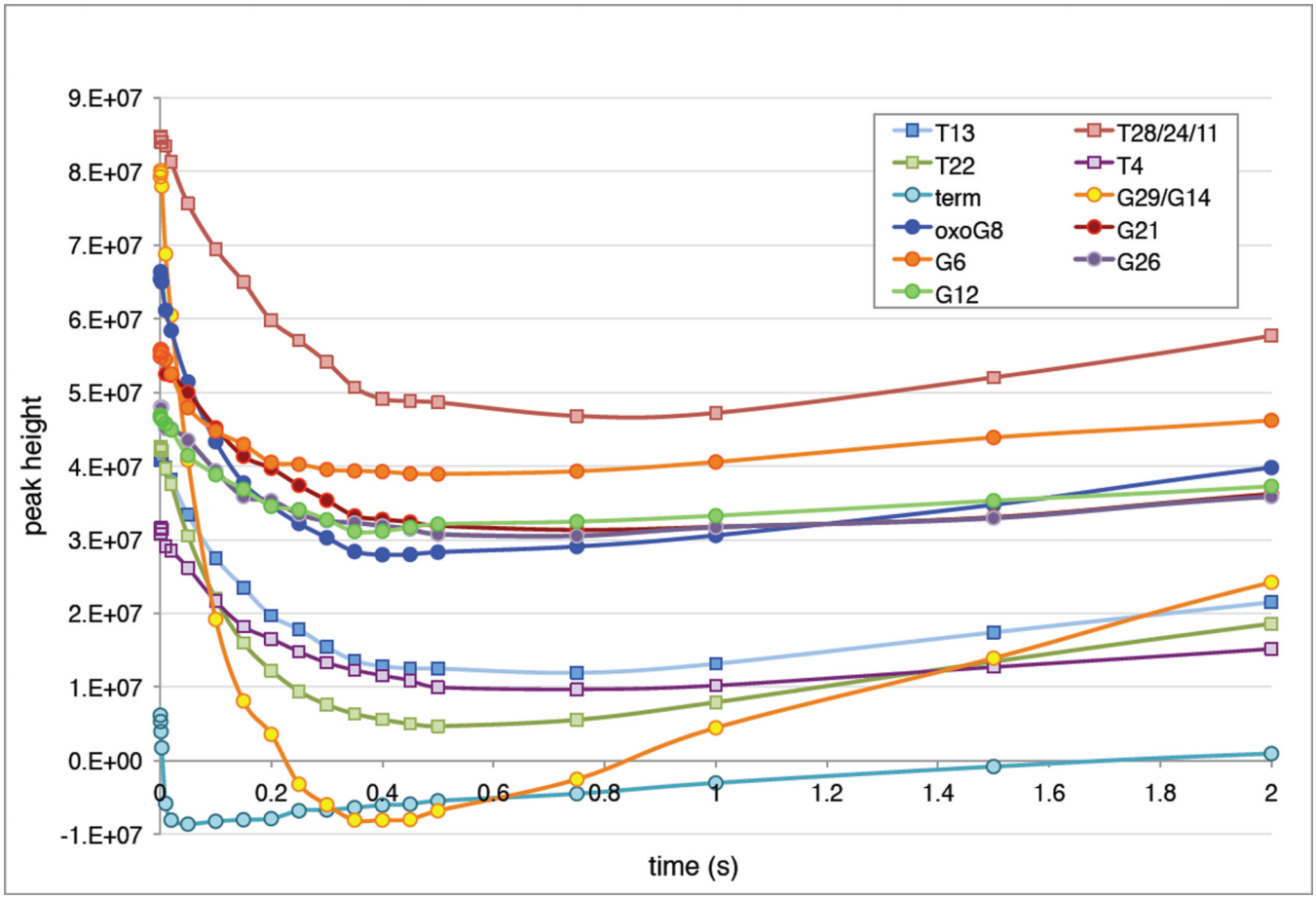

Figure 6. Imino proton intensity as a function of time after selective inversion of water protons

Peak heights as a function of mixing time for lesion duplex **1oxo-2** in the absence of exchange catalyst. The peak intensities decrease modestly as the imino protons exchange with inverted water protons, and then increase as they relax back to their equilibrium value. The curves were fit to Eqn. 4 to determine the exchange rate of the imino proton.

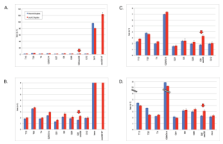

Figure 7. Exchange rate of DNA imino protons at three concentrations of glycine catalyst

In each histogram, the k_{ex} values for base imino protons in the parent (blue) and 8oxoG lesion duplexes (red) are shown in pairs. (A) 5 mM total glycine (12.5 μM active glycine base catalyst) illustrating the exchange rate of one of the terminal peaks and the 8oxoG N7 imino proton, both of which are quite accessible to solution and exchange much more quickly than the internal imino protons. (B) 5 mM total glycine (12.5 μM base) with the y-axis adjusted to illustrate the exchange rates of the internal imino protons. (C) 100 mM total glycine (250 μM base). (D) 1000 mM total glycine (2.5 mM base).

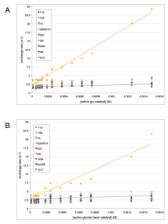

Figure 8. Imino exchange rates in parent and lesion duplexes

The exchange rates of individual protons are shown as a function of glycine catalyst concentration. Guanine imino protons are indicated with circles (G_8/8oxoG_8 in blue) and thymine imino protons with squares. (A) Exchange rate of imino protons in the parent duplex **1–2** between 12.5 μM and 2.5 mM base catalyst. Best-fit lines to Eqn. 8 of the G_{29}/G_{14} exchange rates and G_8 exchange rates are shown. (B) Exchange rate of imino protons in the lesion duplex **1oxo-2** between 12.5 μM and 2.5 mM base catalyst. Best-fit lines to eqn. 8 of the G_{29}/G_{14} exchange rates and 8oxoG_8 exchange rates are shown.

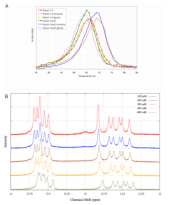

Figure 9. Effect of glycine titrant on DNA stability and structure

(A) 1st derivatives of UV melting curves for parent and lesion duplexes at 5 μM duplex concentration with either no added catalyst, 100 mM glycine, or 100 mM ammonia. (B) Glycine-dependent changes in the imino proton chemical shift in the parent duplex **1–2**.

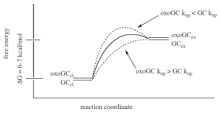

Figure 10. Reaction coordinate diagram illustrating exchange from the G-C and 8oxoG-C base pairs

The free energy difference between the closed state (GC_{cl} and $oxoGC_{cl}$) and the "open" state available for imino proton exchange (GC_{ex} and $oxoGC_{ex}$) is 6–7 kcal/mol, due to the cost of breaking three hydrogen bonds and unstacking one or both bases from the hydrophobic core of the helix. The two base pairs are shown with similar stabilities in both closed and exchangeable states because every method used in this study has found the oxoG-C base pair to be almost indistinguishable from G-C. Critically, many other open forms are likely to exist along the reaction coordinate pathway with similar or higher energies to GC_{ex} and $oxoGC_{ex}$, but these are not shown because they are not directly probed by this experiment. Dashed lines illustrate the effect of increasing or decreasing k_{op} on the activation energy of base pair opening; the latter would extend the lifetime of the open state, and the former would decrease the activation energy of opening.

Table 1

Sequences of the 15 bp DNA Oligonucleotide Duplexes.[†]

*Parent Duplex **1–2***	
Strand 1	5'- C_1 C_2 A_3 T_4 C_5 G_6 A_7 **G_8** A_9 C_{10} T_{11} G_{12} T_{13} G_{14} C_{15} -3'
Strand 2	3'- G_{30} G_{29} T_{28} A_{27} G_{26} C_{25} T_{24} C_{23} T_{22} G_{21} A_{20} C_{19} A_{18} C_{17} G_{16} -5'
*Lesion Duplex **1oxo-2***	
Strand 1oxo	5'- C_1 C_2 A_3 T_4 C_5 G_6 A_7 **oG_8** A_9 C_{10} T_{11} G_{12} T_{13} G_{14} C_{15} -3'
Strand 2	3'- G_{30} G_{29} T_{28} A_{27} G_{26} C_{25} T_{24} C_{23} T_{22} G_{21} A_{20} C_{19} A_{18} C_{17} G_{16} -5'

[†]Nucleotides are numbered sequentially from the 5' end of each strand, indicated with subscripts. Location of the 8-oxoguanine lesion, fortuitously at position #8, is designated by oG.

Table 2

Base Pair Exchange and Opening Parameters[†]

	$\alpha K_{op} \times 10^6$		$k_{int} \times 10^{-6}$, M^{-1} s^{-1}	
	duplex 1–2	**duplex 1oxo-2**	**duplex 1–2**	**duplex 1oxo-2**
G_{29}/G_{14}	35 ± 2	22 ± 3	0.068 ± 0.005	0.15 ± 0.03
G_8 or oxoG_8	1.8 ± 0.4	1.6 ± 0.6	0.87 ± 0.2	1.7 ± 0.6
G_{21}	1.7 ± 0.5	1.1 ± 0.4	0.81 ± 0.2	1.6 ± 0.6
G_6	2.2 ± 0.5	1.3 ± 0.7	1.0 ± 0.2	2.1 ± 1.1
G_{26}	2.4 ± 0.5	2.8 ± 0.7	0.81 ± 0.2	0.81 ± 0.2
G_{12}	0.77 ± 0.3	0.97 ± 0.4	2.4 ± 0.9	2.1 ± 0.8
T_{13}	4.8 ± 0.3	3.1 ± 0.7	0.38 ± 0.02	0.70 ± 0.2
T_4	0.84 ± 0.2	1.0 ± 0.4	2.1 ± 0.5	1.9 ± 0.8

[†] αK_{op}= the apparent equilibrium constant for base pair opening; k_{int} = the intrinsic rate of imino proton exchange, M^{-1} s^{-1}.